A functionalised nickel cyclam catalyst for CO_2 reduction: electrocatalysis, semiconductor surface immobilisation and light-driven electron transfer

Gaia Neri,[a,b] James J. Walsh,[a,b] Calum Wilson,[b] Anna Reynal,[c] Jason Y. C. Lim,[c] Li Xaoe,[c] Andrew J. P. White,[c] Nicholas J. Long,[c] James R. Durrant[c] and Alexander J. Cowan[b]

Electronic supplementary information

Contents:

3.4 Spectroelectrochemistry of TiO_2 and $Ti_{0.8}Zr_{0.2}O_2$ films

3.5 $Ti_{0.8}Zr_{0.2}O_2$ TAS and spectroelectrochemical data

1. Experimental:

1.1 Materials: 1,4,8,11-tetraazacyclotetradecane-6-carboxylic acid was purchased from Chematech. All other starting materials including 4,8,11-tetraazacyclotetradecane, $NiCl_2.6H_2O$ and solvents for the synthesis were purchased from Sigma Aldrich, Fisher Scientific or VWR and were used without further purification unless otherwise specified. Milli-Q water (18.2 MΩ) was used for all aqueous solutions. CO_2 and argon (CP grade) were purchased from BOC. Helium (N6.0) was purchased from BOC. The calibrant gas for the GC was a custom ordered mixture of 500 ppm H_2 and 200 ppm CO in helium and was purchased from STG.

1.2 Apparatus: All electrochemistry was performed using a PalmSens^3 potentiostat. Gas chromatography was performed using an Agilent 6890N employing N6 helium as the carrier gas (5 ml.min^{-1}). A 5 Å molecular sieve column (ValcoPLOT, 30 m length, 0.53 mm ID) and a pulsed discharge detector (D-3-I-HP, Valco Vici) were employed. CO and H_2 peak areas were quantified with multiple calibrant gas injections and were re-calibrated daily. ESI-MS and elemental analyses were performed by the University of Liverpool analytical services. FTIR samples were prepared by depositing a TiO_2 film (*vide infra*) on a CaF_2 slide followed by dipping in a 2 mM solution of **2** in ethanol for 48 hours. FTIR spectra were recorded with a Bruker Vertex 70V Fourier-transform infrared spectrometer using a MIR globar source, KBr beamsplitter and a liquid nitrogen-cooled HgCdTe detector, at a resolution of 2 cm^{-1}. ATR-FTIR measurements of the powder were carried out on a Nicolet iS50 FTIR (with iS50 ATR attachment) spectrometer (Thermo Fisher Scientific) using reflectance mode in a N_2 filled glove box. Profilometry was measured using an Ambios Technology XP200. UV-Vis spectra were recorded on a Shimadzu UV-2600 spectrophotometer.

Spectroelectrochemical measurements were performed in a homemade PTFE cell with quartz windows, using an Autolab potentiostat (PGSTAT12) to apply voltage while measuring the absorption of the sample with a Perkin Elmer Lambda 35 UV/vis spectrophotometer. A three-electrode configuration was employed, with a nanostructured film deposited onto FTO as working electrode, a Pt wire as the counter electrode and a Ag/AgCl (sat. KCl) reference electrode (E^0 = + 0.197 V vs. NHE). The absorption of the

semiconductors as a function of the voltage applied was monitored at λ_{abs} = 780 nm, corresponding to the absorption of electrons in the conduction band of TiO_2 and $Ti_{0.8}Zr_{0.2}O_2$.

Scanning electron microscopy (SEM) images were obtained with a Philips XL-30 field emission gun scanning electron microscope. Samples were coated with Au (2 nm) prior to observation. SEM was used to determine the morphology of the $Ti_{0.8}Zr_{0.2}O_2$ particles and films. The thickness of the mesoporous nanostructured films was 4 μm, measured by profilometry (Tencor Instruments). The $Ti_{0.8}Zr_{0.2}O_2$ particles had a diameter of ~ 20 nm. X-Ray diffraction (XRD) measurements were made on a Philips PW1710 diffractometer with monochromatic Cu radiation.

The microsecond-second transient absorption decays were measured using a Nd:YAG laser (Big Sky Laser Technologies Ultra CFR Nd:YAG laser system, 6 ns pulse width). The third harmonic of the laser, corresponding to 355 nm, at a frequency of 1 Hz, was used as the excitation pulse. Typical excitation densities of 350 μJ/cm^2 were used, unless otherwise stated. A liquid light guide with a diameter of 0.5 cm was used to transmit the laser pulse to the sample. The probe light source was a tungsten lamp (Bentham IL1 tungsten lamp) and the probing wavelength was selected by using a monochromator OBB-2001 dual grating, Photon Technology International) placed prior to the sample. Transient absorption data were collected with a Si photodiode (Hamamatsu S3071). The information was passed through an amplifier box (Costronics) and recorded using a Tektronics TDS 2012c oscilloscope (microsecond to millisecond timescale) and a National Instruments (NI USB-6211) DAQ card (millisecond to second timescale). The decays observed are the average between 500 and 1000 laser pulses. The data was processed using home-built software based on Labview.

1.3 Synthesis of catalysts: [Ni(cyclam)]Cl_2 (**1**) was prepared according to literature procedures.[1]

[Ni(cyclam-CO_2H)]Cl_2 (**2**): $NaHCO_3$ (250 mg, 3 mmol) was added to a solution of 1,4,8,11-tetraazacyclotetradecane-6-carboxylic acid (130 mg, 0.5 mmol) in water (10 ml). When gas evolution had stopped, $NiCl_2 \cdot H_2O$ (130 mg, 0.55 mmol) was added. The mixture turned orange in a matter of minutes, and was stirred at room temperature for two hours. The solvent was evaporated to dryness under reduced pressure. The residual solid was dissolved in ethanol (20 ml) and the pale-green powder was filtered off, to give a light purple solution. The solvent was evaporated to dryness and the mauve, crystalline solid thus obtained was dried under vacuum overnight. Obtained: 83 mg, yield 45 %; **ATR-IR**: 3184 (br), 2915, 2856, 1580 (s), 1451, 1400, 1390, 1365, 1090, 945, 879 cm^{-1}; **ESI-MS**: 301 [M^+-2Cl]; **CHN**

microanalysis: Anal. calcd. for $C_{11}H_{24}Cl_2N_4NiO_2 \cdot 0.5H_2O \cdot 0.5C_2H_5OH$: C, 35.50; H, 6.95; N, 13.80. Found: C, 35.45; H, 6.68; N, 14.03.

1.4 Film preparation: Films for electrochemistry: Anatase TiO_2 films[2] were prepared by depositing TiO_2 colloidal paste (average particle diameter = 20 nm) on fluorine-doped tin oxide (FTO) slides. The slides were sonicated in ethanol for 20 minutes before deposition. The paste was deposited on the films and spread with a glass rod. The thickness was controlled by using scotch tape and was measured *via* profilometry to be an average of 3 μm. The films were allowed to dry before the slides were heated at 450°C for 30 minutes. The slides were cut so that the geometric surface area of the TiO_2 films was 1 cm^2.

Films for TAS: Anatase TiO_2 and $Ti_{0.8}Zr_{0.2}O_2$ films were deposited onto microscope or fluorine-doped tin oxide (FTO) coated glass from their respective colloidal pastes using the doctor-blading technique and calcined in a furnace at 450°C for 30 min. The anatase TiO_2 paste was prepared as described in the literature.[2] $Ti_{0.8}Zr_{0.2}O_2$ colloidal paste was prepared as follows:[3] Acetic acid (2.4 g) and titanium isopropoxide ($Ti(iPrO)_4$, 10.53 mL), were mixed under nitrogen with vigorous stirring (700 rpm) until a pale yellow colour appeared. $Zr(iPrO)_4$ ($Zr(iPrO)_4$–IPA, 3.45 g) pre-dissolved in 16 mL anhydrous isopropanol solution was added. After stirring for 10 min, the mixture was poured into a conical flask containing 63 mL of 0.1 M HNO_3 solution at room temperature. The resulting milky mixed oxide suspension was subsequently stirred at 80°C for 8 h. Finally, the mixture was poured into a Teflon inlet inside a stainless steel reactor and heated at 240°C for 12 h. Polyethylene glycol (PEG) 20,000 (50% of $Ti_{1-x}Zr_xO_2$ by weight) was added to the above colloidal solution to prevent subsequent film cracking during heat treatment and to enhance film porosity.

Immobilization of the catalyst on the TiO_2 films was obtained by dip-coating the slides in a 2 mM solution of **2** in EtOH for 48 hours, followed by thorough rinsing with ethanol. The adsorption of the catalyst was monitored by UV-Vis spectroscopy.

1.5 Electrocatalysis: The electrolyte used for aqueous electrochemistry was $NaClO_4$. The solutions were adjusted to pH 5 by addition of either NaOH or $HClO_4$. TiO_2 film electrochemistry was carried out in dry acetonitrile (spectrophotometric grade, ≥ 99.5 %, Sigma Aldrich) with tetra-*n*-butylammonium hexafluorophosphate, $(But)_4NPF_6$, as the supporting electrolyte. Cyclic voltammograms of the catalyst in solution were carried out in a pear-shaped flask with a hanging mercury drop working electrode (geometric surface area = 0.023 cm^2, measured by averaging the weight of several drops and accounting for the density of mercury), or a glassy carbon disk working electrode (BASi, geometric surface area = 0.0717 cm^2). A Pt coil was used as the counter electrode and a Ag/AgCl (3 M NaCl) as the

reference electrode (BASi). The flask was purged with either argon or CO_2 for 20 minutes prior to experiments. Controlled potential electrolysis (CPE) was performed in a custom made pyrex H-cell with the two compartments separated by a fine glass frit. The working electrode was a mercury/gold amalgam wire freshly prepared for each experiment. A 80 x 0.5 mm gold wire (Goodfellow) was polished with fine grit polishing pad (BASi) and rinsed with water and acetone. When dry, it was dipped in a mercury pool for 3 minutes and the excess mercury was removed. The geometric surface area of the electrode was estimated to be ~ 2.54 cm^2, approximately half of which was submerged in the electrolyte solution during experiments. The wire was recovered after each experiment by dipping the electrode in concentrated nitric acid for 30 seconds and rinsing with water several times and then with acetone. The counter electrode was kept in the second compartment to minimise re-oxidation of CO or other reaction products. Both compartments were magnetically stirred throughout the CPE reaction. Results presented are based on an average of at least two independent measurements, with typical variability of ~ ± 10 % in product yields. The Faradaic efficiencies (FE) achieved were calculated by taking the measured product yields (by GC headspace analysis) and charge passed (Q) and accounting for the requirement of 2 electrons to produce one CO molecule.

$$FE_{CO}\ (\%) = \left[\frac{\mathrm{CO}\ (mol)}{\left[Q(C) \Big/ 2 \times 96485\ (C\ mol^{-1}) \right]} \right] \times 100$$

$$TON_{CO} = \frac{\mathrm{CO}\ (mol)}{electroactive\ catalyst\ (mol)}$$

2. Catalyst Characterisation

2.1 CV of solution phase of $[Ni(cyclam\text{-}CO_2H)]^{2+}$ on GCE

A glassy carbon electrode was employed to study the $Ni^{II/III}$ couple as it sits outside the electrochemical window for a HMDE. The Ag/AgCl conversion has been estimated from the known potential of the Fc/Fc^+ couple in pure acetonitrile, Fig S1.[4] For completeness we also report the behaviour of the $Ni^{II/I}$ couple under both Ar and CO_2 on a GCE in an acetontitrile water mix, fig S3, S4.

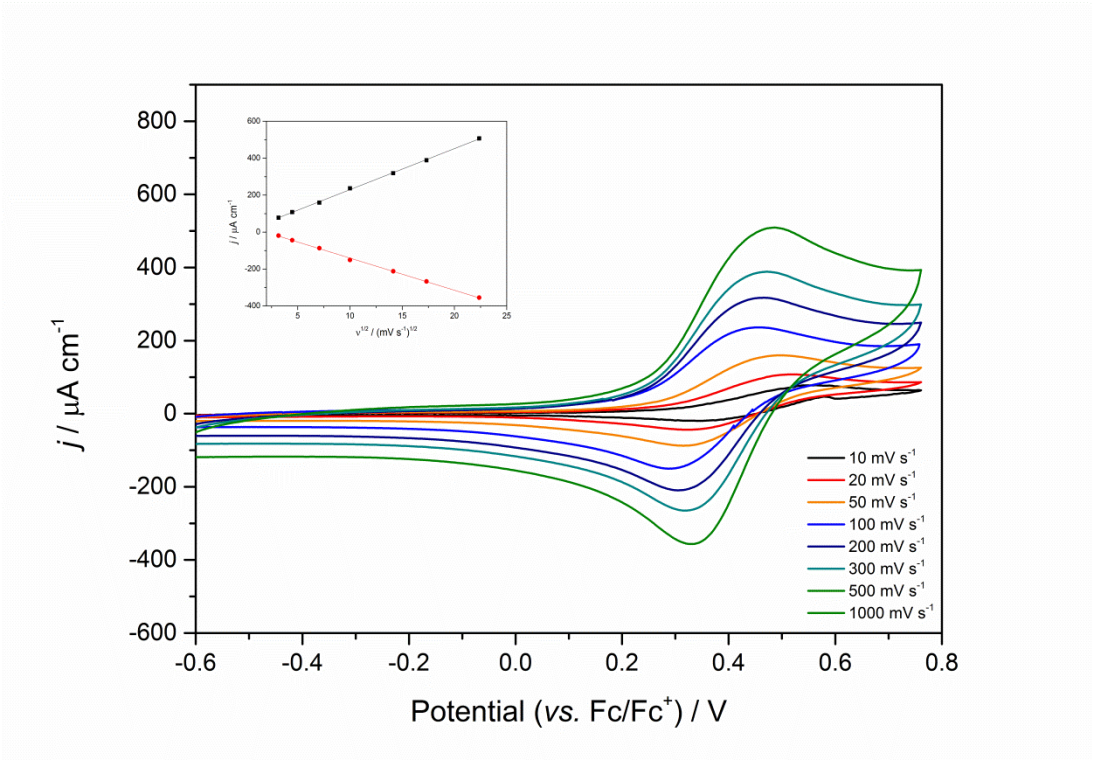

*Figure S1: CVs at positive potentials for an Argon-purged 1 mM solution of **2** in MeCN doped with 10 % water, using 0.1 M $(But)_4NPF_6$ as the supporting electrolyte and a GCE. The inset shows the dependence of the peak current with the square root of the scan rate, demonstrating diffusion-controlled, reversible behaviour.*

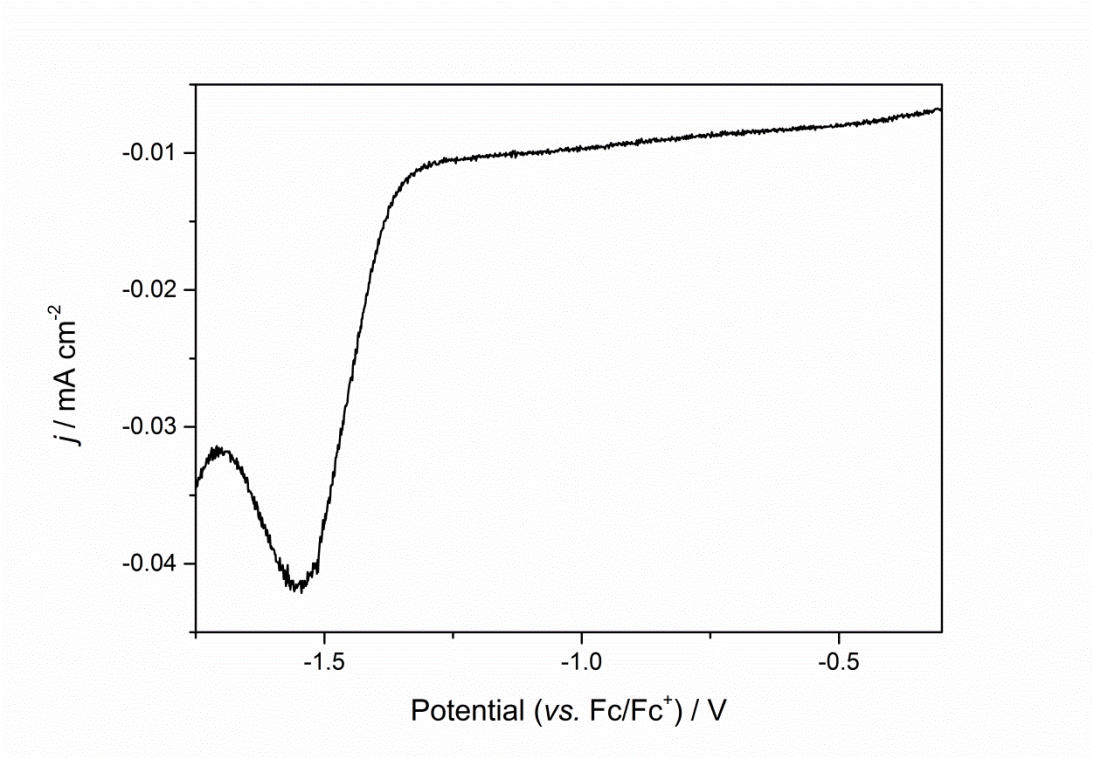

*Figure S2: Squarewave voltammetry of an Argon-purged 1 mM solution of **2** in MeCN with 10 % added water, using 0.1 M $(But)_4NPF_6$ as the supporting electrolyte and a GCE.*

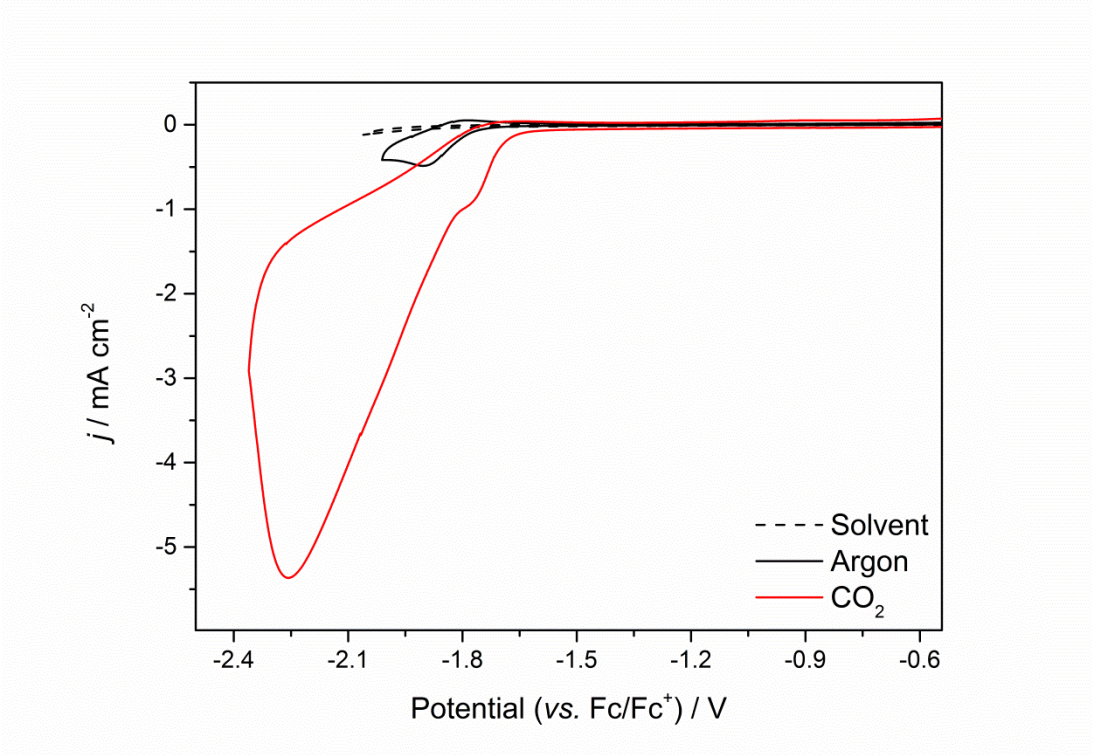

Figure S3: CVs of 1 mM $[Ni(cyclam\text{-}CO_2H)]^{2+}$ in MeCN with 10 % added water, using 0.1 M $(But)_4NPF_6$ as the supporting electrolyte and a GCE, under both argon and CO_2.

2.2 CV of solution phase of $[Ni(cyclam\text{-}CO_2H)]^{2+}$ on HMDE under argon

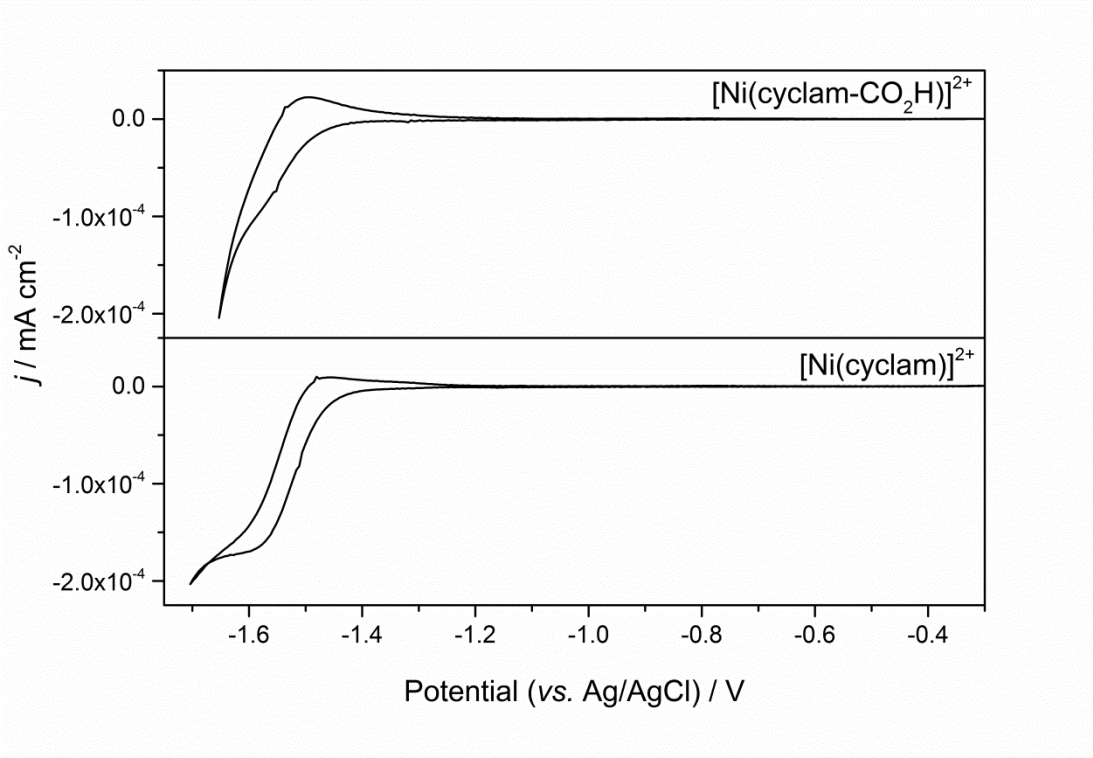

Figure S4: CVs of 1 mM $[Ni(cyclam\text{-}CO_2H)]^{2+}$ in Ar-purged H_2O containing 0.1 M $NaClO_4$ on a HMDE working electrode. v = 100 mV/s.

2.3 Scan rate dependence on HMDE

The scan rate dependence of the $Ni^{II/I}$ couple on a HDME in the presence of both Argon (S5) and CO_2 (S6) is shown below.

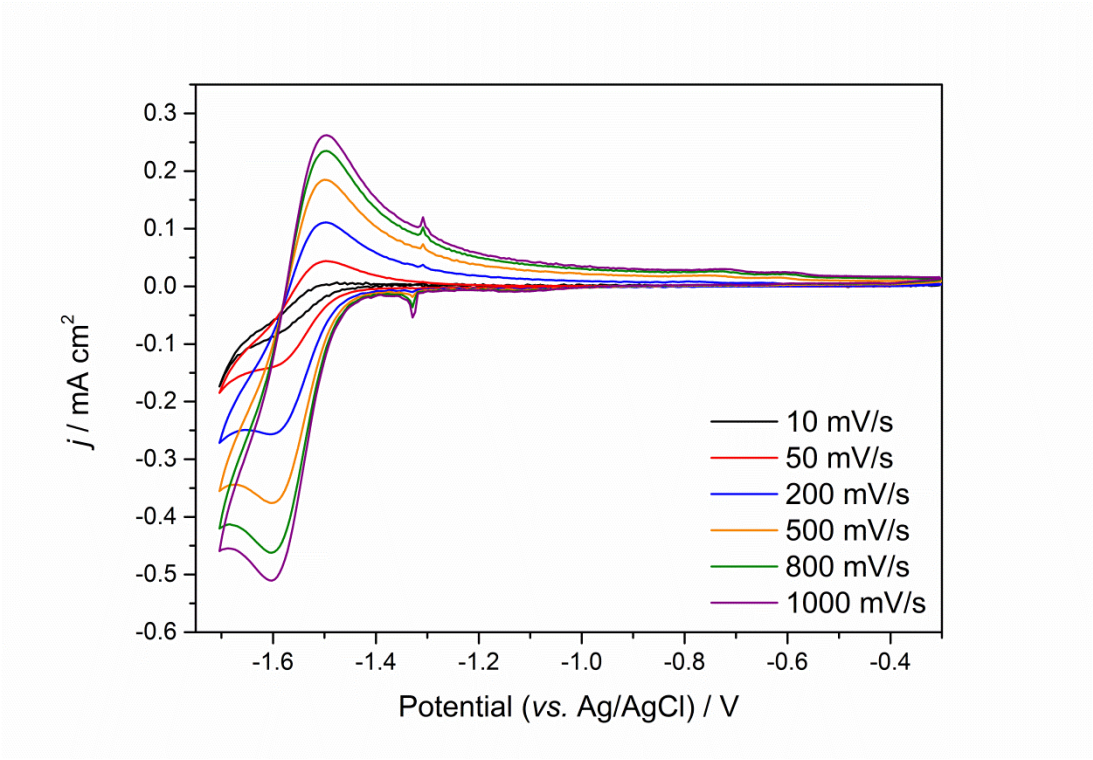

Figure S5: CVs of 1 mM $[Ni(cyclam\text{-}CO_2H)]^{2+}$ in Ar-purged H_2O containing 0.1 M $NaClO_4$ on a HMDE working electrode at increasing scan rates.

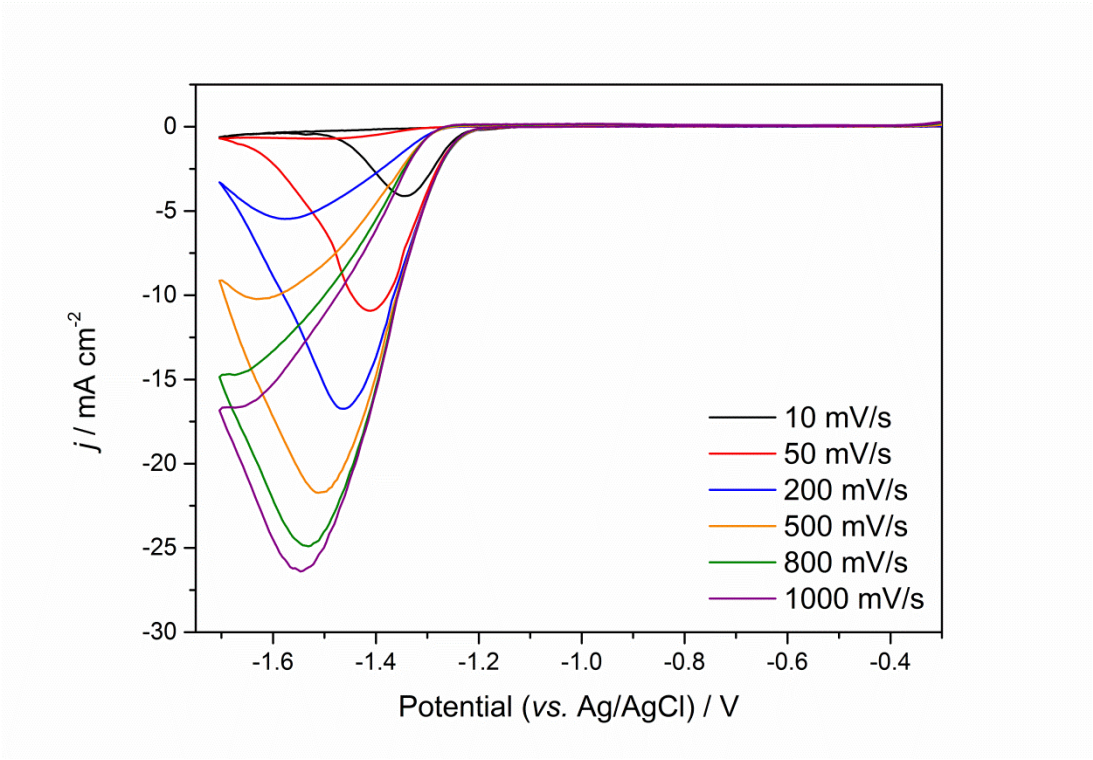

Figure S6: CVs of 1 mM [Ni(cyclam-CO_2H)]$^{2+}$ in CO_2-purged H_2O containing 0.1 M $NaClO_4$ on a HMDE working electrode at increasing scan rates.

2.4 CPE of [Ni(cyclam-CO_2H)]$^{2+}$ on Au-Hg amalgam electrode

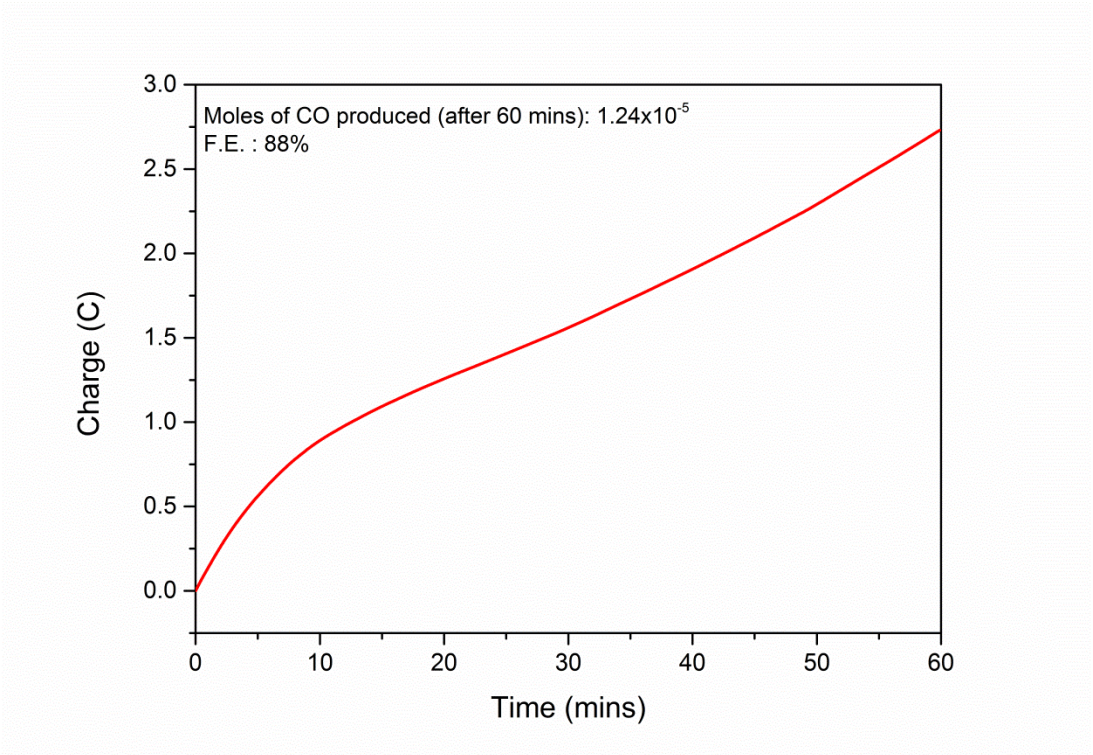

*Figure S7: CPE of a 1 x 10^{-4} M solution of **2** containing 0.1 M $NaClO_4$, pH 5. Potential was poised at -1.4 V for 1 hour using a Au-Hg amalgam electrode.*

2.5 Spectroscopic characterization of $[Ni(cyclam\text{-}CO_2H)]^{2+}$

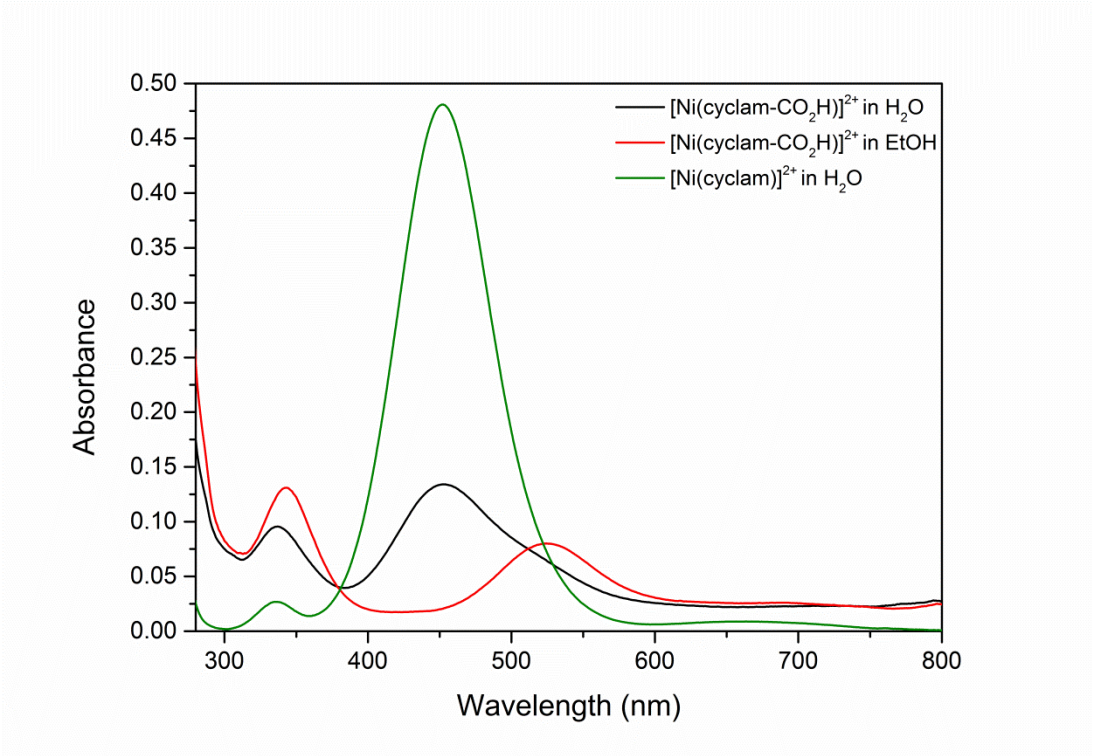

Figure S8: Solution UV-Vis spectra of $[Ni(cyclam)]^{2+}$ (10 mM in H_2O) and $[Ni(cyclam\text{-}CO_2H)]^{2+}$ (10 mM in both ethanol and water).

It is well established[5-9] that nickel complexes of tetraazamacrocycles exist in solution as an equilibrium mixture of their high-spin and low-spin states. Spin interconversion causes a definite change of the coordination geometry. In $[Ni(cyclam)]^{2+}$ the high-spin state corresponds to a distorted octahedral geometry, with two solvent molecules occupying the axial site of a distorted octahedron, whereas the low-spin state corresponds to a square planar geometry. This equilibrium has been shown to be highly dependent on temperature, solvent and on the nature of the complex counterion. For $[Ni(cyclam)]^{2+}$ in water at 25°C the square planar geometry dominates, with a major absorption peak at 452 nm and a shoulder at 335 nm. The UV-Vis of **2** in water presents three major absorption peaks at 526, 453 and 337 nm, respectively, characteristic of mixed geometry, which is in line with previous studies of nickel macrocyclic complexes. Interestingly when the complex is solubilised in ethanol the peak at 452 nm disappears and the absorption spectrum changes to one typical of a 6 coordinate species, with peaks at 525 and 342 nm.

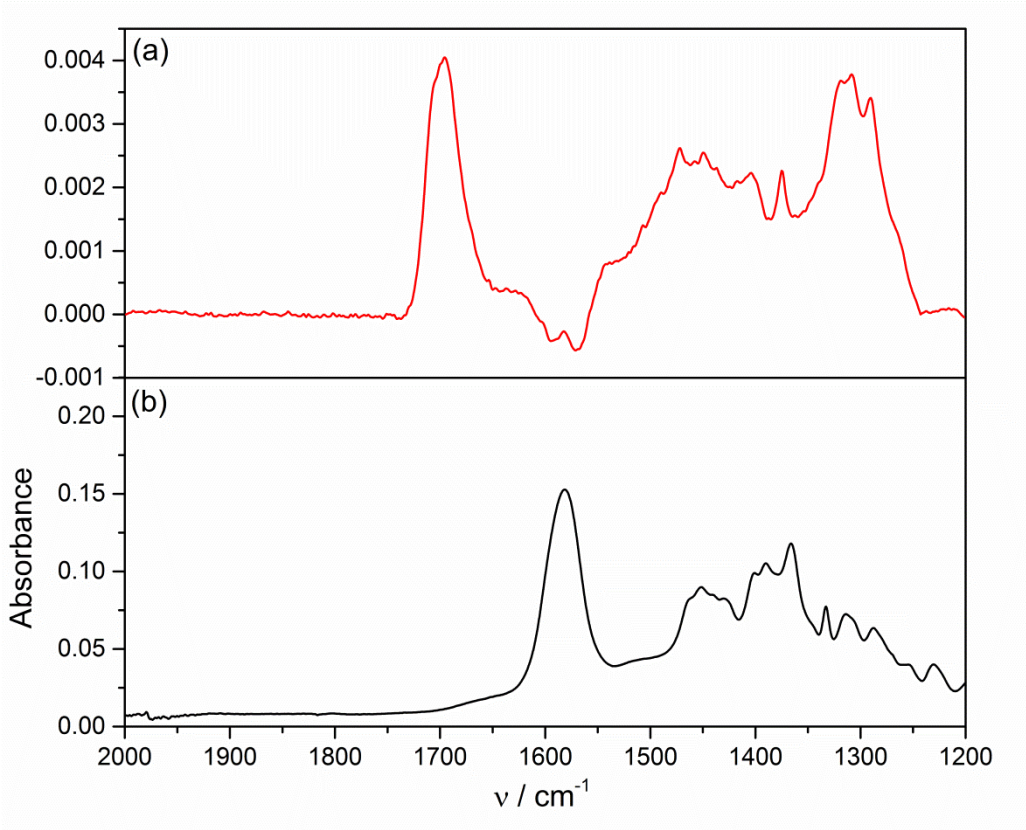

*Figure S9: (a) FTIR absorbance spectrum for a TiO_2 film on a CaF_2 slide modified with **2**; (b) ATR-FTIR absorbance spectrum of catalyst **2** powder.*

The ATR-FTIR of free **2** reveals the absence of a symmetrical CO stretching mode at approximately 1700 cm^{-1}. Instead, the spectrum is dominated by the $\nu_{as}(CO_2^-)$ stretch at 1580 cm^{-1}, with the $\nu_s(CO_2^-)$ stretch visible at 1375 cm^{-1}. The absence of a C=O functionality strongly implies that **2** exists as a carboxylate salt in the solid state.[10] In contrast, the spectrum (absorbance mode) of **2** on TiO_2 shows the presence of a C=O symmetrical stretching mode at 1696 cm^{-1}. The asymmetric and symmetric $\nu_{as}(CO_2^-)$ and $\nu_s(CO_2^-)$ modes were observed at 1583 and 1375 cm^{-1}, respectively. The peak separation $\nu_{as\text{-}s}$, characterized by $\nu_{as}(CO_2^-)$ - $\nu_s(CO_2^-)$, can be used to assess the binding mode of a carboxylate group to a TiO_2 surface according to the empirical rule that band separation follows $\nu_{as\text{-}s}$ (monodentate) > $\nu_{as\text{-}s}$ (isolated) > $\nu_{as\text{-}s}$ (bidentate).[11] The band splitting for **2** on TiO_2 was 208 cm^{-1}, larger than the 197 cm^{-1} for the free complex, which implies monodentate surface co-ordination. This is contrast to the binding of a carboxylic acid modified $[Co(cyclam)]^{2+}$ derivative to TiO_2 reported previously *via* a bidentate mode.[12]

2.6 Crystallographic data

The X-ray crystal structure of 2

***Crystal data for* 2**: $C_{11}H_{24}Cl_2N_4NiO_2 \cdot H_2O$, M = 391.97, monoclinic, $P2_1/n$ (no. 14), a = 6.66207(9), b = 17.0552(2), c = 15.01109(19) Å, β = 102.4162(13)°, V = 1665.71(4) Å^3, Z = 4, D_c = 1.563 g cm^{-3}, μ(Cu-Kα) = 4.767 mm^{-1}, T = 173 K, pale purple blocks, Oxford Diffraction Xcalibur PX Ultra diffractometer; 3260 independent measured reflections (R_{int} = 0.0239), F^2 refinement,[13] R_1(obs) = 0.0365, wR_2(all) = 0.1031, 2954 independent observed absorption-corrected reflections [$|F_o| > 4\sigma(|F_o|)$, $2\theta_{max}$ = 145°], 219 parameters. CCDC 1028579.

The seven N–H and O–H hydrogen atoms in the structure of 2 were found from ΔF maps and refined freely subject to N–H and O–H distance constraints of 0.90 Å.

3. Film characterization

3.1 TiO_2 cyclic voltammetry

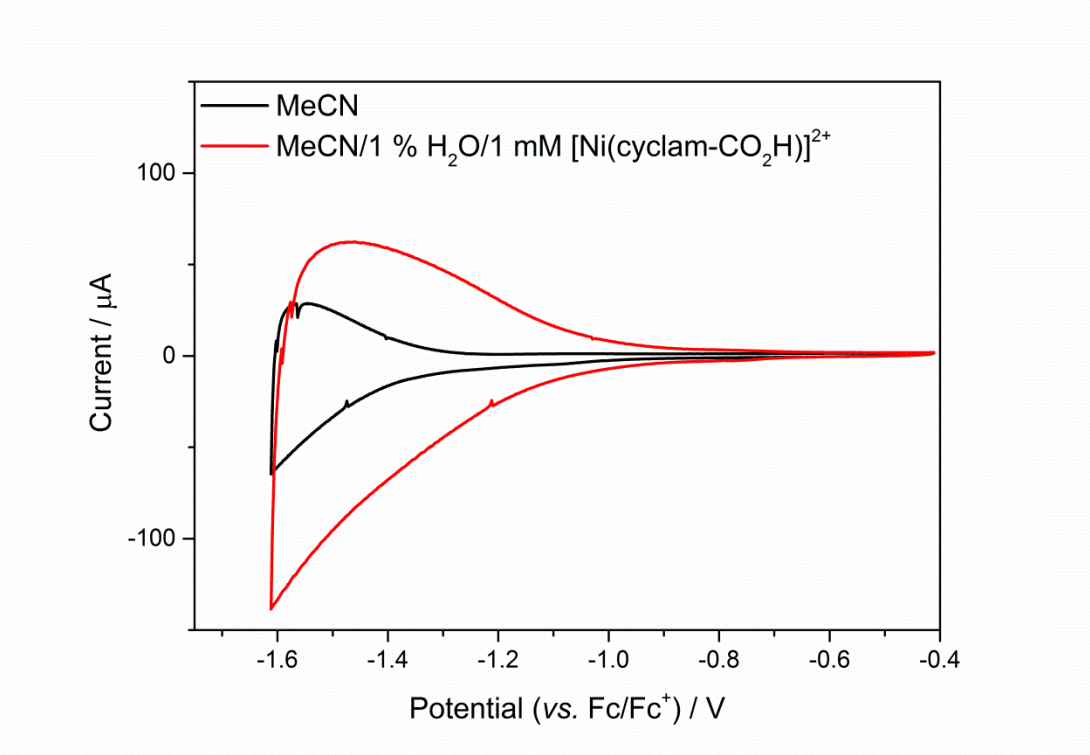

Figure S10: CVs of a TiO_2 electrode in blank MeCN (black) and following addition of ***2*** *in H_2O (red) to make a 1 mM solution of* ***2*** *in MeCN/1 % water The data show the shift in the charge/discharge behaviour upon increasing the proton concentration, but no additional reduction curve corresponding to $Ni^{II/I}$ reduction in solution. Supporting electrolyte was 0.1 M $(But)_4NPF_6$.*

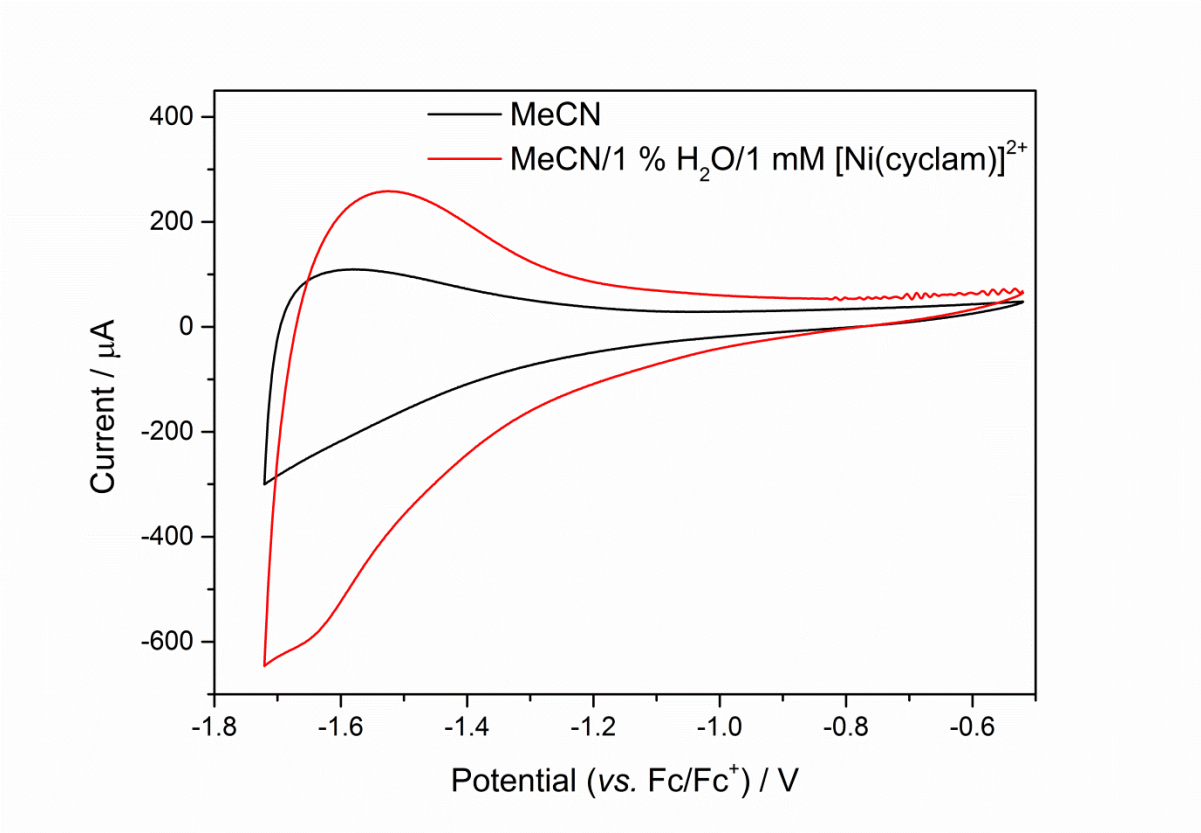

Figure S9: CVs of a TiO_2 electrode in blank MeCN (black) and following addition of ***1*** *in H_2O (red) to make a 1 mM solution of* ***1*** *in MeCN/1 % water. The data show the shift in the charge/discharge behaviour upon increasing the proton concentration, but no additional reduction curve corresponding to $Ni^{II/I}$ reduction in solution. Supporting electrolyte was 0.1 M $(But)_4NPF_6$.*

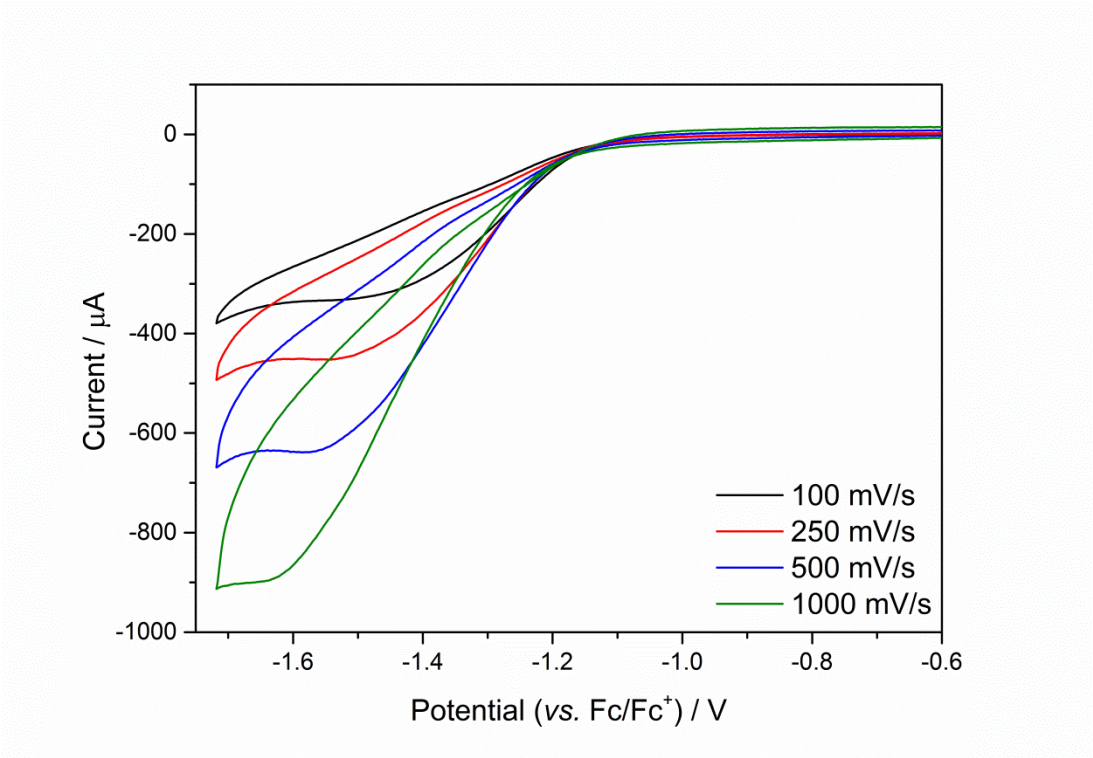

*Figure S12: Scan rate dependence of **2** on a TiO_2 electrode in Argon-purged MeCN/0.1 M $(But)_4NPF_6$.*

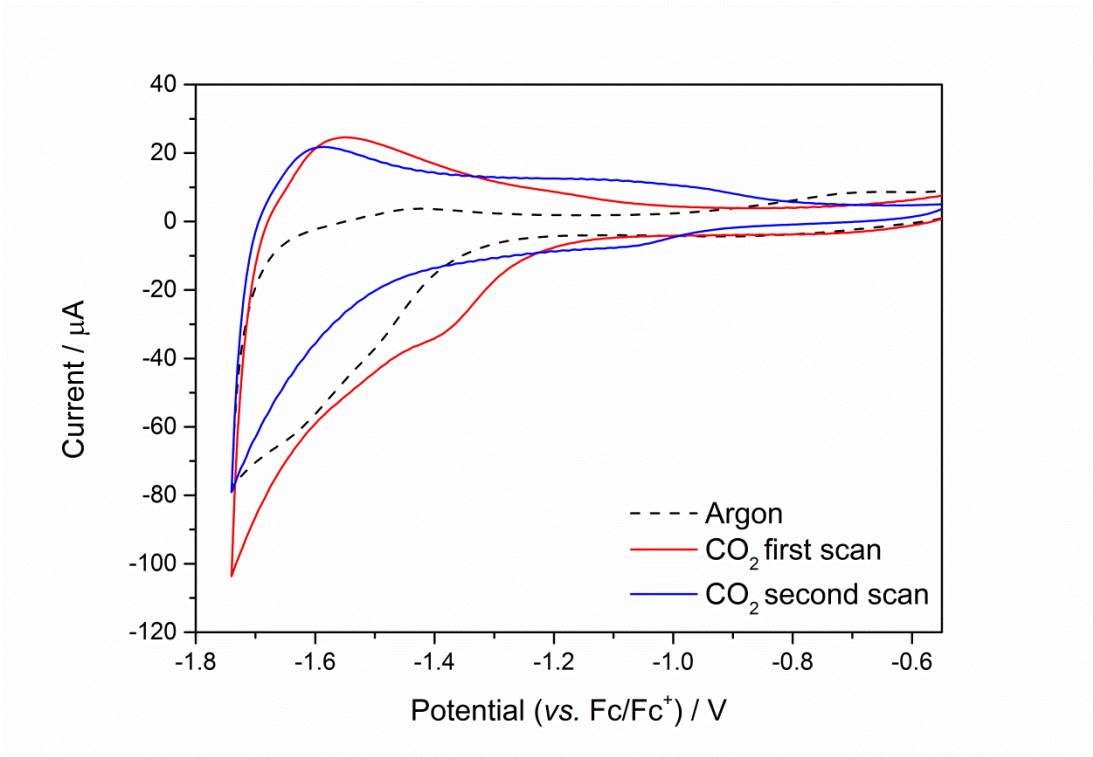

*Figure S13: CVs of a TiO_2/**2** electrode in MeCN under argon (black) and CO_2 (red, first scan; green, second scan). The data show the initial increase in the current. On subsequent scans, however, the reductive feature assigned to the nickel disappears and the curve takes the shape of a blank TiO_2 film. This behaviour is attributed to the poor stability of the*

complex bond to the semiconductor under CO_2. The supporting electrolyte was 0.1 M $(But)_4NPF_6$.

3.2 Adsorption experiments

The quantity of catalyst adsorbed on the TiO_2 surface was calculated using a recently reported method by soaking a **2**-modified film in 1 M NaOH solution for 4 hours and comparing the UV-Vis to that of a 2 mM solution of **2** in 1 M NaOH.[14] For a 6 x 1 cm film with a thickness of 3 μm the number of molecules adsorbed was found to be 1.7 x 10^{17}.[14] The number of TiO_2 particles in the film was found by taking into account the average radius of the nanoparticles and the volume of the film.

The volume of one particle is: $\frac{4}{3}\pi(10x10^{-9})^3 = 4.2x10^{-24}m^3$

The volume of the film is $A_{film} \cdot L_{film} \cdot (1 - P_{film}) = 6x10^{-4}m^2 \cdot 3x10^{-6}m \cdot (1 - 0.6) = 7.2x10^{-10}m^3$

The ratio between the volume of the film and the volume of one particle thus gives the total number of particles in the film: $\#_{particles} = \frac{7.2x10^{-10}}{4.2x10^{-24}} = 1.7x10^{14}$

The surface coverage is given by the total number of molecules adsorbed divided by the total number of nanoparticles in the film: $\frac{1.7x10^{17}}{1.7x10^{14}} = 1000\ molecules/nanoparticle$

3.3 XRD and SEM of TiO_2, ZrO_2 and $Ti_{0.8}Zr_{0.2}O_2$ films

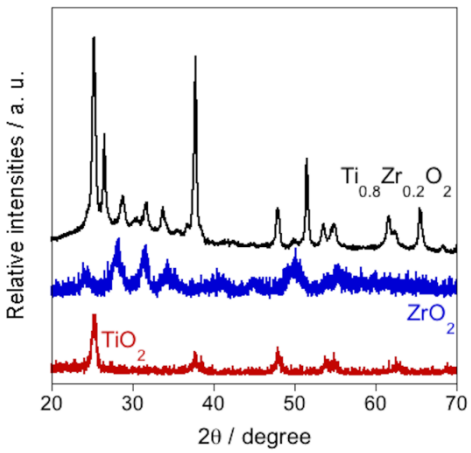

Figure S14. X-ray diffraction (XRD) patterns of TiO_2 (red trace), ZrO_2 (blue trace) and $Ti_{0.8}Zr_{0.2}O_2$ (black trace) films.

$Ti_{1-x}Zr_xO_2$ materials are known to behave as solid solutions only until the solubility of zirconium in the TiO_2 lattice reaches a maximum; after this threshold extra zirconium is present only as ZrO_2. Reports on the solubility of zirconium on TiO_2 vary from a minimum of x = 0.08 to x = 0.35.[15, 16] Here we have prepared a solution with x = 0.2; it is clear from the XRD pattern that there is some contribution from ZrO_2, however the shift in the conduction band edge observed in the spectroelectrochemical data (*vide infra*) suggests the presence of some percentage of solid solution in the material prepared.[3]

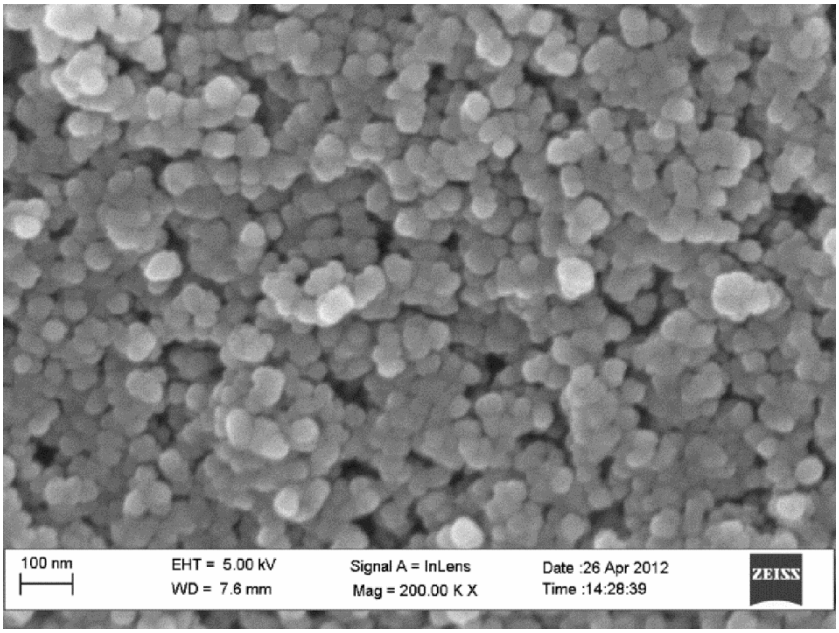

Figure S15: Scanning Electron Micrograph of a $Ti_{0.8}Zr_{0.2}O_2$ film, showing a particle size of ca. 20 nm.

3.5 $Ti_{0.8}Zr_{0.2}O_2$ TAS and spectroelectrochemical data

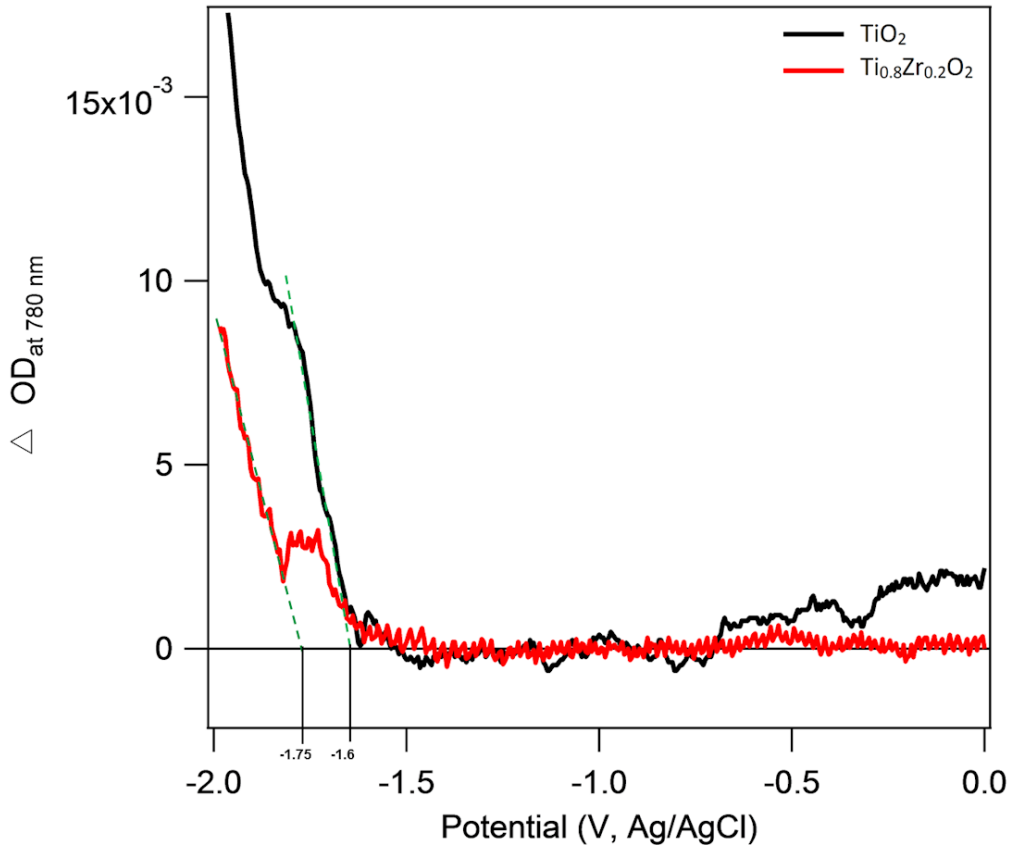

Figure S16: Absorbance at 780 nm as a function of applied potential for TiO_2 and $Ti_{0.8}Zr_{0.2}O_2$ electrodes, in MeCN with $(But)_4NPF_6$ 0.1 M as the supporting electrolyte.

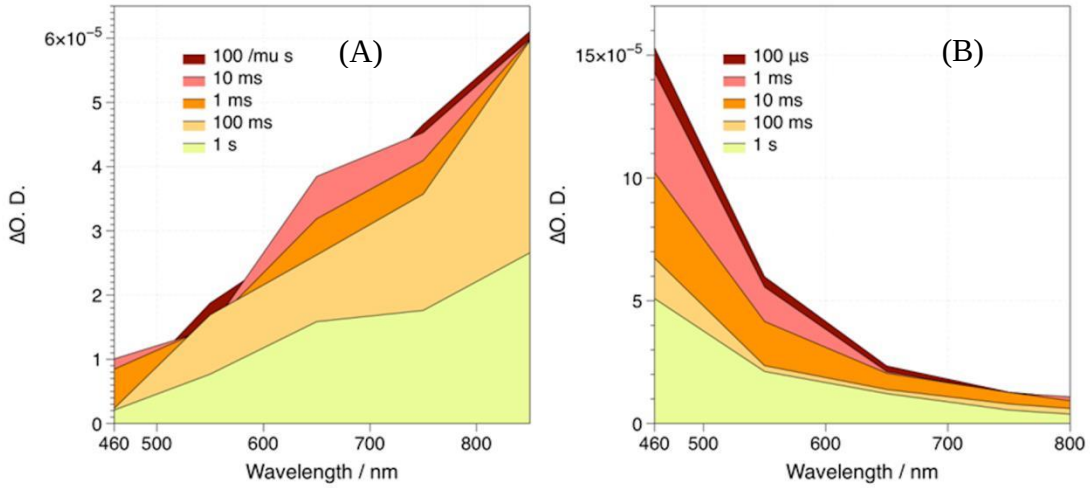

Figure S17. Transient absorption spectra of (a) photoexcited electrons in a $Ti_{0.8}Zr_{0.2}O_2$ film using methanol as the hole scavenger, and (b) $Ti_{0.8}Zr_{0.2}O_2$ holes, when employing a 10^{-3} M $AgNO_3$ aqueous solution as the electron scavenger. The samples were excited at 355 nm with a laser intensity of 350 $\mu J/cm^2$ and a repetition rate of 1 Hz.

Semiconductor	Conduction Band Edge[a] (V_{Fc/Fc^+})	TiO_2/**2** $Ni^{II/I}$ (V_{Fc/Fc^+})	ΔG (eV, *estimated*[b])	$t_{50\%}$ (s)[c]
nc-TiO_2	-2.0	-1.5	-0.5	$1.2x10^{-3}$
$TiO_{0.8}Zr_{0.2}$	-2.15	-1.5	-0.65	$0.8x10^{-3}$

Table S1: Potentials of electron transfer processes. [a] *Estimated from the onset of the 780 nm absorption edge by spectroelectrochemistry in $CH_3CN/(But)_4NPF_6$ (Figure S16).* [b] *Assuming that the reduction potential of **2** is not significantly altered upon binding to $TiO_{0.8}Zr_{0.2}$ when compared to TiO_2.* [c] *Rate of photoelectron transfer from semiconductor to molecular catalyst, measured by TAS (Fig 5).*

References

1. J. D. Froehlich and C. P. Kubiak, *Inorg. Chem.*, 2012, **51**, 3932-3934.
2. S. Ito, T. N. Murakami, P. Comte, P. Liska, C. Grätzel, M. K. Nazeeruddin and M. Grätzel, *Thin Solid Films*, 2008, **516**, 4613-4619.
3. M. Durr, S. Rosselli, A. Yasuda and G. Nelles, *J Phys Chem B*, 2006, **110**, 21899-21902.
4. V. V. Pavlishchuk and A. W. Addison, *Inorg. Chim. Acta*, 2000, **298**, 97-102.
5. B. Bosnich, M. L. Tobe and G. A. Webb, *Inorg. Chem.*, 1965, **4**, 1109-1112.
6. A. Anichini, L. Fabbrizzi, P. Paoletti and R. M. Clay, *Inorg. Chim. Acta*, 1977, **24**, L21-L23.
7. L. Y. Martin, C. R. Sperati and D. H. Busch, *J. Am. Chem. Soc.*, 1977, **99**, 2968-2981.
8. E. J. Billo, P. J. Connolly, D. J. Sardella, J. P. Jasinski and R. J. Butcher, *Inorg. Chim. Acta*, 1995, **230**, 19-28.
9. M. Boiocchi, L. Fabbrizzi, F. Foti and M. Vazquez, *Dalton T.*, 2004, 2616-2620.
10. D. A. Long, *Journal of Raman Spectroscopy*, 2004, **35**, 905-905.
11. C. Bauer, G. Boschloo, E. Mukhtar and A. Hagfeldt, *J. Phys. Chem. B*, 2002, **106**, 12693-12704.
12. P. V. Bernhardt, G. K. Boschloo, F. Bozoglian, A. Hagfeldt, M. Martinez and B. Sienra, *New Journal of Chemistry*, 2008, **32**, 705-711.
13. G. Sheldrick, *Acta Crystallographica Section A*, 2008, **64**, 112-122.
14. A. Reynal, J. Willkomm, N. M. Muresan, F. Lakadamyali, M. Planells, E. Reisner and J. R. Durrant, *Chem. Commun.*, 2014, **50**, 12768-12771.
15. J. C. Yu, J. Lin and R. W. M. Kwok, *J. Phys. Chem. B*, 1998, **102**, 5094-5098.
16. B. F. Gao, Y. Ma, Y. A. Cao, Z. J. Gu, G. J. Zhang and J. N. Yao, *Chinese J. Chem.*, 2007, **25**, 484-489.